Image formation by nuclear magnetic resonance: The sensitivepoint method

Waldo S. Hinshaw

Citation: Journal of Applied Physics **47**, 3709 (1976); doi: 10.1063/1.323136
View online: http://dx.doi.org/10.1063/1.323136
View Table of Contents: http://scitation.aip.org/content/aip/journal/jap/47/8?ver=pdfcov
Published by the AIP Publishing

Image formation by nuclear magnetic resonance: The sensitive-point method*

Waldo S. Hinshaw†

Department of Physics, University of Pittsburgh, Pittsburgh, Pennsylvania 15260
(Received 17 June 1975)

An image formation method, using nuclear magnetic resonance techniques, has been developed which provides direct and detailed information on the interior details of heterogeneous samples. Time-dependent magnetic field gradients are used to limit and control the region of spatial sensitivity of a standard pulsed NMR spectrometer. A continuous string of intense phase-alternated rf pulses is used to provide a continuous monitor of the nuclear magnetization. The image is produced by directly plotting the phase-detected resonance signal on a xy plotter as the limited region of spectrometer sensitivity is scanned through the sample. An analysis of the method in terms of the phenomenological Bloch equations, a description of the experimental method, and a representative selection of images are presented. A spatial resolution of about 0.3 mm has been achieved.

PACS numbers: 07.70., 33.90.

I. INTRODUCTION

Since its inception, nuclear magnetic resonance has become an important and powerful research tool. Recently interest has been growing in applying the techniques of NMR to biological problems. This interest has been spurred by the realization that the proton relaxation times of healthy and cancerous tissues are different.[1–5] The application of NMR to biological problems has been hindered by the fact that the technique can measure only the spatially averaged properties of the sample. In order to compare the properties of healthy and cancerous tissue, for example, the samples must be excised and placed separately in the spectrometer. This process injures the subject from which the samples were taken and often alters the properties to be measured.[6,7]

Lauterbur has recently produced images of the distribution of resonant nuclei in heterogeneous samples using a method he has named the "zeugmatographic" technique.[8–10] Other researchers are beginning to use this technique and related methods to produce similar images.[11–17] NMR zeugmatography is based on the fact that the resonance spectrum of a sample in an inhomogeneous magnetic field is broadened in a manner which depends upon the shape of the sample. If the intensity of the magnetic field changes uniformly with distance across the sample and the direction of the field is constant, an otherwise narrow line is broadened and corresponds to a projection of the sample. An image of the sample is produced by combining the spectra, or projections, recorded for several gradient directions. The reconstruction process is similar to the reconstruction algorithms developed for electron microscopy and other fields.[18] Using this basic zeugmatographic technique and variations of it, Lauterbur has been able to measure the sample density and T_1 relaxation time as a function of position in the sample.

This paper describes a simple method of rendering the NMR spectrometer sensitive to only one point within the sample. Preliminary aspects of the method have been described elsewhere.[19,20] Time-dependent field gradients are applied to the sample in such a manner that only one point of the sample experiences a time-independent field. The signal from this one "sensitive point" is selected by recording only the time-independent component of the total signal. This technique makes it possible to measure sample density, relaxation times, macroscopic flow, and other quantities at any selected point in the sample and thus provides a means for applying many of the powerful techniques of NMR to heterogeneous samples.

The general sensitive-point technique is a method of specializing to one point and not necessarily a method of image formation as is conventional zeugmatography. In this work, however, the sensitive-point technique is used to produce images, or zeugmatograms, of the spatial distribution of the sample. The signal induced by the nuclear magnetization of the sample at the sensitive point is continually monitored as the point is slowly and systematically moved through the sample. This signal is plotted on an xy plotter which is scanned synchronously with the sensitive point.

The sensitive-point method of image formation has distinct advantages over the more conventional methods of zeugmatography. (i) The demands made upon the uniformity of the magnetic field are much weaker. The difficult problem of producing uniform gradient fields is avoided since the spatial accuracy of the image depends only on the accuracy with which the location of the sensitive point is known, not on the linearity of the gradients. For the same reason, nonuniformities in the static resonant magnetic field have no effect on the image as long as the intensity of the field in the region of the sensitive point obeys the Larmor condition. (ii) A small region of the sample can be investigated without acquiring equivalent data from the remainder of the sample. For example, a direct measurement of the T_1 relaxation time can be made at an accurately selected point in the sample. (iii) The point-by-point method of image formation is simple and direct. The inherently inexact and time-consuming computational process of image reconstruction is not required.

The ideas underlying the sensitive-point method of image formation are discussed in Sec. II. Section II A describes the rf pulse sequence used to provide a continuous monitor of the bulk nuclear magnetization. The response of the magnetization to this pulse sequence is calculated from the Bloch equations. Section II B dis-

cusses the time-dependent field gradients and the resulting spatial restriction of the spectrometer sensitivity. Section II C attempts to describe the result of combining the pulses and gradients. Section III describes, in some detail, the equipment used to produce the images. Section IV presents a few images selected to demonstrate the capabilities of the technique. Section V discusses the limitations and possibilities of the sensitive-point method of image formation.

II. METHOD

A. Pulses

Carr observed that a continuous resonance signal could be obtained by subjecting a sample to a continuous string of intense rf pulses.[21] The rf pulses were near the Larmor frequency and the interpulse interval was short compared to the relaxation times of the sample. This pulse technique, which Carr called "steady-state free precession", will be referred to in this paper as the SFP technique. The SFP technique produces a relatively large and continuous resonance signal and thus is ideal for the sensitive-point imaging application. Other properties of the SFP technique of particular value to this application will be mentioned later. A modification of the SFP technique, designed to enhance very weak NMR signals, has been reported in the literature.[22]

The phenomenological Bloch equations[23] can be used to describe the resonance signal produced by the SFP technique and to describe the effect of time-dependent gradients upon the signal. For simplicity, the Bloch equations are first solved for a constant and uniform magnetic field, H_0. For a sample with gyromagnetic ratio γ, the Bloch equations of motion for the magnetization, M, can be written

$$\frac{d\mathbf{M}}{dt} = \gamma \mathbf{M} \times \mathbf{H}_e - (M_x \hat{j} + M_y \hat{j})/T_2 - (M_z - M_0)\hat{k}/T_1 \qquad (1)$$

with

$$\mathbf{H}_e \equiv (H_0 - \omega/\gamma)\hat{k} + H_1 \hat{i}.$$

Here $\hat{i}$, $\hat{j}$, and $\hat{k}$ are the unit vectors of a frame rotating with frequency ω about the common z axis of the laboratory frame. H_0 is in the z direction, and the rf field, H_1, is in the x direction of the rotating frame. Equation (1) is solved for two cases. During the rf pulse, H_1 is much larger than $H_0 - \omega/\gamma$ and relaxation effects are negligible. A pulse of length τ rotates $\mathbf{M}$ through an angle $\alpha \equiv \gamma H_1 \tau$ about the x axis. Using the rotation operator P, the effect of the rotation on the magnetization can be written

$$\mathbf{M}(\tau) = P(\tau)\mathbf{M}(0), \qquad (2)$$

where

$$P(\tau) \equiv \begin{pmatrix} 1 & 0 & 0 \\ 0 & \cos\alpha & \sin\alpha \\ 0 & -\sin\alpha & \cos\alpha \end{pmatrix}.$$

Between pulses, the solution of Eq. (1) is

$$\mathbf{M}(t) = R(t)\mathbf{M}(0) + M_0[1 - \exp(-t/T_1)]\hat{k}, \qquad (3)$$

where the operator R is given by

$$R(t) \equiv \begin{pmatrix} \exp(-t/T_2)\cos\delta\omega t & \exp(-t/T_2)\sin\delta\omega t & 0 \\ -\exp(-t/T_2)\sin\delta\omega t & \exp(-t/T_2)\cos\delta\omega t & 0 \\ 0 & 0 & 1 \end{pmatrix}$$

with the definitions $\delta\omega \equiv \omega_0 - \omega$ and $\omega_0 \equiv \gamma H_0$.

The effect on the magnetization of one "pulse cycle", defined here as an interval of length T followed by a rf pulse of length τ, is obtained by combining Eqs. (2) and (3). If the magnetization at the end of the pulse cycle is denoted by $\mathbf{M}^+$ then

$$\mathbf{M}^+ = P(\tau)R(T)\mathbf{M}(0) + M_0(1 - E_1)P(\tau)\hat{k}, \qquad (4)$$

where $E_1 \equiv \exp(-T/T_1)$ and $\mathbf{M}(0)$ is the magnetization at the start of the cycle. If a train of identical pulses is maintained for a time long compared to T_1, the behavior of the magnetization during any one pulse cycle must be the same as that during any other. Thus the magnetization at the beginning of each pulse cycle must be the same, a condition which can be written $\mathbf{M}(0) = \mathbf{M}^+$. If this "steady-state" condition is applied to Eq. (4) and the result solved for the magnetization just after each pulse, $\mathbf{M}^+$, then

$$\mathbf{M}^+ = M_0(1 - E_1)[P^{-1}(\tau) - R(T)]^{-1}\hat{k} \qquad (5)$$

or

$$\mathbf{M}^+ = Q \begin{pmatrix} E_2 \sin\alpha \sin\beta \\ \sin\alpha(1 - E_2\cos\beta) \\ \cos\alpha(1 - E_2\cos\beta) + E_2(E_2 - \cos\beta) \end{pmatrix} \qquad (6)$$

with

$$Q \equiv \frac{M_0(1 - E_1)}{(1 - E_1\cos\alpha)(1 - E_2\cos\beta) - (E_1 - \cos\alpha)(E_2 - \cos\beta)E_2}$$

and with the definitions $E_2 \equiv \exp(-T/T_2)$ and $\beta \equiv \delta\omega T$.

Here $\mathbf{M}^+$ is the magnetization, expressed in the rotating frame, just after each pulse with the system in the steady-state condition. The behavior of the magnetization during the interval between pulses is given by Eq. (3) with $\mathbf{M}(0)$ replaced by $\mathbf{M}^+$. Equation (6) has been derived elsewhere in the literature for the problem of pulsed Fourier transform NMR.[24,25]

Equation (6) clearly shows the ability of the SFP technique to produce a relatively strong and continuous NMR signal. For simplicity, assume that 90° rf pulses are used and that $T_1 = T_2$. Then for the y component of $\mathbf{M}^+$, Eq. (6) gives

$$M_y^+ = M_0 \frac{1 - E_1\cos\beta}{1 + E_1(1 - \cos\beta) + E_1^2}. \qquad (7)$$

If the rf pulses are applied at the Larmor frequency, ω_0, and if the interpulse interval is short compared to the relaxation time, then, with the approximation $E_1 = 1 - T/T_1$, Eq. (7) becomes

$$M_y^+ = M_0 T/2T_1.$$

Thus closely spaced 90° pulses applied at the Larmor frequency produce a very small signal. However, if the rf pulses are not at the Larmor frequency but off resonance by an amount $\delta\omega = k\pi/T$, where k is an odd

integer, then, for closely spaced pulses, Eq. (7) becomes

$$M_y^+ = \tfrac{1}{2}M_0.$$

Thus half of the full equilibrium magnetization, M_0, is continually in the xy plane. This transverse magnetization produces the relatively large and continuous resonance signal which makes the sensitive-point imaging technique viable.

A variety of experimental schemes can be employed to observe the signal induced in the sample coil by the transverse magnetization M_y^+. In his original work on SFP, Carr used diode detection.[21] Preliminary images have been produced using the same technique but with phase-sensitive detection.[19] The phase-detector reference frequency and the rf pulse frequency were identical and differed from the Larmor frequency by an amount $\delta\omega = \pi/T$. For the work reported here, however, the rf pulses differ in phase from one to the next by 180°. The phase-detector reference frequency, the rf pulse frequency, and the Larmor frequency are the same.

Phase alternating the rf pulses is an experimentally convenient way to fulfill the condition, $\delta\omega = k\pi/T$, necessary for the success of the SFP technique. If the rf pulses are short compared to the interpulse interval, a string of phase-alternated pulses of frequency ω is equivalent to a string of nonphase-alternated pulses of frequency $\omega + k\pi/T$. Thus phase-alternated rf pulses at the Larmor frequency satisfy the condition $\delta\omega = k\pi/T$.

Equations equivalent to Eqs. (3) and (6), but describing the behavior of the magnetization in the presence of phase-alternated rf pulses, could be obtained by considering a pulse cycle containing two pulses and two intervals and following the same development used to obtain the earlier equations. It is easier to rewrite Eqs. (3) and (6), transforming them from a frame rotating at frequency ω, in which all rf pulses are in the x direction, to a frame rotating at frequency $\omega' = \omega + k\pi/T$, in which, if k is an odd integer, alternate pulses are in the positive and negative x directions. In performing this coordinate transformation, we let an arbitrary pulse in the pulse train be at $t=0$ and let the two rotating reference frames coincide at $t=0$. Denote by $\mathbf{m}_n^+$ the magnetization, expressed in the frame rotating at frequency ω', just after the rf pulse at $t=nT$, where n is an integer. Thus at $t=0$, we obtain $\mathbf{m}_0^+ = \mathbf{M}^+$, and just after the pulse at $t=nT$ we obtain

$$\mathbf{m}_n^+ = \begin{pmatrix} (-1)^n & 0 & 0 \\ 0 & (-1)^n & 0 \\ 0 & 0 & 1 \end{pmatrix} M^+. \tag{8}$$

Thus Eq. (6) becomes, with the variables $\delta\omega$ and β expressed in terms of the equivalent new variables $\Delta\omega \equiv \omega_0 - \omega'$ and $\phi = \Delta\omega T$,

$$\mathbf{m}_n^+ = q \begin{pmatrix} -(-1)^n E_2 \sin\alpha \sin\phi \\ (-1)^n \sin\alpha\,(1 + E_2 \sin\phi) \\ \sin\phi(1 + E_2 \sin\phi) + E_2(E_2 + \sin\phi) \end{pmatrix}, \tag{9}$$

where q is identical to Q but with $\cos\beta$ replaced by $-\sin\phi$. The equivalent transformation of Eq. (3) gives the time dependence of the magnetization expressed in the frame rotating at frequency ω',

$$\mathbf{m}_n(t) = r(t')\mathbf{m}_n^+ + M_0[1 - \exp(-t'/T_1)]\hat{k}, \tag{10}$$

where the operator $r(t)$ is identical to $R(t)$ with $\delta\omega$ replaced by $\Delta\omega$. In this equation, $(t - nT)$ has been replaced by t' for simplicity. The equation is valid for $0 \le t' \le T$ or, equivalently, $nT \le t \le (n+1)T$. Equation (10) gives the response of the bulk nuclear magnetization to a continuous string of phase-alternated rf pulses and can be used to calculate the signal produced by the phase-alternated SFP technique.

If phase-sensitive detection is used with reference frequency ω', the NMR signal is proportional to one of the transverse components of $\mathbf{m}_n(t)$. For this work, the phase detector was adjusted to be sensitive to the y component of the magnetization. The y component is the "in-phase" component since the x component of $\mathbf{m}_n(t)$ is zero when $\Delta\omega = 0$. By combining Eqs. (9) and (10), the y component of $\mathbf{m}_n(t)$ can be written

$$m_{ny}(t) = (-1)^n q \sin\alpha \exp(-t'/T_2)[\cos\Delta\omega t' + E_2 \cos\Delta\omega(T - t')]. \tag{11}$$

The equivalence of t' and $T - t'$ in this equation, which obtains for $T \ll T_2$, results in the formation of echoes before each pulse if inhomogeneous broadening is considered. A second point of interest about this expression for $m_{ny}(t)$ is that n appears explicitly only in the term $(-1)^n$. Thus the NMR signal after each pulse alternates in sign but is otherwise unchanged. This alternation is a significant advantage in applications such as sensitive-point imaging where long-term signal averaging is required. By removing the signal alternation at the last signal handling stage of the experimental system, the entire spectrometer operates as a "chopper stabilized" amplifier. The problems of baseline drift and low-frequency noise are removed.

In recording the NMR signal for the sensitive-point application, the detected signal is time averaged, or integrated, after the sign alternation is removed. Thus the recorded signal is proportional to f_y where

$$f_y = (1/T)\int_0^T (-1)^n m_{ny}(t)\,dt. \tag{12}$$

In order to maximize the integrated signal amplitude, the interpulse interval is much shorter than the relaxation times. Performing the integral in Eq. (12) and then taking the limit of fy as T/T_1 and T/T_2 go to zero while the ratio T_1/T_2 remains constant gives

$$f_y = \frac{2M_0 \sin\phi \sin\alpha}{\phi[(1+\cos\alpha)(1+\cos\phi) + 2(1-\cos\alpha)T_1/T_2]}. \tag{13}$$

This is the continuous time-independent signal predicted by the Bloch equations for the pulse technique used in this experiment. Here α is the angle through which the magnetization is rotated by each pulse and ϕ is the resonance frequency offset times the pulse interval.

One advantage of the SFP technique for the sensitive-point imaging application is the weak dependence of the

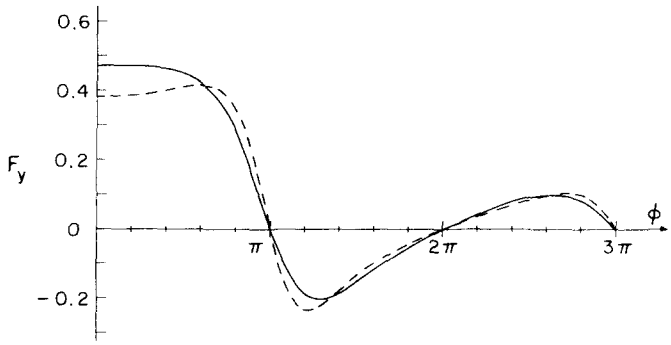

FIG. 1. Calculated resonance signal, f_y, in units of the equilibrium magnetization, M_0, as a function of $\phi \equiv \Delta\omega T$ for the phase-alternated SFP technique. The solid and broken lines are for 70° and 50° rf pulses, respectively. The curves were calculated from Eq. (13) with $T_1 = T_2$. Note that limited variations in frequency offset and pulse amplitude cause relatively little change in the signal. These curves also represent the spatial response function produced by the SFP technique in the present of a static gradient if ϕ is replaced by $\gamma G x T$.

signal amplitude upon both H_1 and H_0. The insensitivity of f_y to H_1 can be shown by setting $\phi = 0$ in Eq. (13), which then becomes

$$f_y = \frac{M_0 \sin\alpha}{T_1/T_2 + 1 - \cos\alpha\,(T_1/T_2 - 1)}. \tag{14}$$

Thus for $T_1 = T_2$, we obtain $f_y = \frac{1}{2} M_0 \sin\alpha$, and any pulse near 90° gives a maximum signal. Equation (14) indicates that the ratio T_1/T_2 can be determined by measuring f_y as a function of α, for example by plotting $\sin(\alpha/f_y)$ as a function of $\cos\alpha$. However, Eq. (14) is predicated on the validity of the Bloch equations and thus should be accepted only as an indication that the signal depends on the relaxation times and pulse angle.

Equation (13) shows that the signal is also relatively insensitive to H_0. If, for simplicity, $\alpha = \frac{1}{2}\pi$ and $T_1 = T_2$, then

$$f_y = 2M_0 \frac{\sin\phi}{\phi} \frac{1}{3 + \cos\phi}. \tag{15}$$

The dependence of f_y upon ϕ, a measure of the resonance offset, is a broad function which is independent of T_2. For $\phi = \frac{1}{2}\pi$, f_y is down from its maximum value of only 15%. The insensitivity of the SFP technique to H_0 is a necessary condition for the success of the sensitive-point technique. If cw techniques were used to induce resonance, for example, the field H_0 would have to be maintained on resonance, or within about $1/\gamma T$ of resonance, over all of the sample and for the duration of the image formation process. The dependence of the signal upon resonance offset for two different rf pulse amplitudes is shown in Fig. 1. The curves were calculated from Eq. (13) with $T_1 = T_2$.

Thus far, only the steady-state situation has been considered. There are situations of interest, however, when the magnetization just after a pulse is not identical to the steady-state value, $\mathbf{M}^+$, as given by Eq. (6). This non-steady-state condition occurs, for example, when the pulse sequence is first turned on or when an additional rf pulse is applied to the system during the continuous pulse train. This kind of non-steady-state situation, with H_0 remaining constant, can be treated by repeated application of Eq. (4), and can be written

$$\mathbf{M}^+_{nT} = (PR)^n(\mathbf{M}^+_0 - \mathbf{M}^+) + \mathbf{M}^+. \tag{16}$$

Here $\mathbf{M}^+_{nT}$ is the magnetization just after the pulse at $t = nT$ and $\mathbf{M}^+_0$ is the magnetization just after the pulse at $t = 0$. The operator PR represents, in physical terms, a shrinking and then a rotation. Equation (16) indicates that the magnitude of vector $\mathbf{M}^+_{nT} - \mathbf{M}^+$ shrinks toward zero and the magnetization tends toward the steady-state value, $\mathbf{M}^+$. For simplicity, assume the sample is on resonance, phase-alternated 90° rf pulses are applied, and T is short compared to T_1 and T_2. For non-steady-state considerations, it is convenient to take the time average of the signal over two adjacent intervals. Let F_{2n} denote the average of the signal f_y for the interval before and the interval after the pulse at $t = 2nT$. With the above assumptions, it can be shown that F_{2n} is given by

$$2F_{2n} = (m^+_y + m^+_z - M_0)\exp(-2nT/T_a) + M_0, \tag{17}$$

where m^+_y and m^+_z are the components of the magnetization just after the pulse at $t = 0$ and where T_a is given by $1/T_a \equiv \frac{1}{2}(1/T_1 + 1/T_2)$.

Equation (17) is similar to the expression for the recovery of the longitudinal magnetization in the absence of the continuous train of rf pulses, and suggests a method for measuring T_1 in liquids where $T_1 = T_2$ and where the Bloch equations are valid. The signal observed after the addition of a 180° pulse to the continuous pulse train at $t = 0$ is

$$F_{2n} = \tfrac{1}{2}[1 - 2\exp(2nT/T_1)]M_0. \tag{18}$$

Thus during the continuous pulse train, the T_1 recovery of the magnetization after a 180° pulse can be directly observed and plotted. The function F_{2n} can be recorded and repeatedly co-added in order to improve the signal-to-noise ratio for weak signals. This method of determining T_1 is well suited to the sensitive-point technique. Streever and Carr[26] reported measuring T_1 by recording the signal produced when the rf pulse string is first turned on. The two methods are similar.

The SFP technique can be considered a "driven equilibrium" method.[27,28] The driven equilibrium Fourier transform, or DEFT, pulse sequence consists of three rf pulses each separated by interval τ with the triplet repeated at much longer intervals T. This sequence can be written (90°, τ, 180°, τ, 90°, T)^n where 90° and 180° are the pulse amplitudes and n is the number of times the triplet is repeated. This triplet sequence has been suggested as a convenient method of monitoring the magnetization after a single 180° pulse and thus measuring T_1 for samples with long T_1 or weak signals.[26,29] However, the method seems to be rarely used, possibly as a result of the accumulated errors introduced by rf inhomogeneity. Various modifications of the triplet sequence designed to remove the rf inhomogeneity problem have been suggested in the literature.[26,30,31] One simple modification, which apparently has not been suggested, is to shift the phase of the center pulse by 180° with respect to the other two. This removes the effect of the rf inhomogeneity and, in fact, little error

is accumulated as long as the amplitudes of the three pulses are in the proportions 1 : 2 : 1. With this phase-alternated triplet, the signal has the opposite sign during the two τ intervals, which is convenient for removing the effect of baseline drift. If the interval between the triplets, T, is reduced to zero, the phase-alternated triplet sequence becomes the phase-alternated SFP technique.

B. Gradients

If a static inhomogeneous magnetic field is applied to a magnetic resonance sample, the resonance spectrum is inhomogeneously broadened. If the intensity of the field, H, varies linearly with position, x, across the sample, then $H(x) = H_0 + Gx$ where H_0 is the homogeneous component and G is the gradient strength. If other broadening mechanisms are negligible, the resonance spectrum, $f(\omega)$, is given by

$$f(\omega) = \int\int \rho(x)\, dy\, dz \tag{19}$$

with

$$x = (\omega/\gamma - H_0)G^{-1},$$

where ρ is the spatial distribution of spins with gyromagnetic ratio γ. Thus the amplitude of the spectrum at a particular frequency is proportional to the number of resonant spins in the corresponding plane of the sample.

If the amplitude of the gradient, G, is time dependent, the resulting spectrum no longer has a simple relationship to the spin distribution. In fact in this situation the spectra obtained by the slow passage cw technique and by taking the Fourier transform of a single free induction decay are different. The spectra obtained by the two techniques are identical for a system with time dependence, such as a time-dependent magnetic field, only if care is taken to perform the same time averaging in both cases. Despite the complications, changing the direction or amplitude of the gradient field during the measurement can provide more spatial information about the sample than is available with a static gradient field. Kumar *et al.*[16] have been able to reconstruct images from the information contained in a set of free induction decays which were produced by applying a 90° rf pulse and a gradient field which was switched in direction at various times during the free induction decay. Others[10,17] have used one gradient field direction during the rf pulse, or sequence of rf pulses, to select a plane in the sample and a second, orthogonal, gradient direction during the free induction decay to determine the distribution of spins in the selected plane. Rough images have also been produced by applying a field gradient which continually changed direction during the free induction decay.[19] This paper, however, is concerned with the decidedly earlier method of using time-dependent field gradients to define a single point in the sample.

If a magnetic field with a linear gradient component which has a time-dependent amplitude is applied to a sample, there is one plane in that sample which experiences a time-independent field. In the following discussion, this plane will be referred to as the "zero-field plane" since the gradient field component is zero in this plane. Also in the following, the time dependence is assumed to be in the gradient amplitude, not in the gradient direction. The gradients referred to are the components of the magnetic field that can be expressed in terms of the quantities $\delta H_z/\delta x$, $\delta H_z/\delta_y$, and $\delta H_z/\delta_z$.

The NMR signal produced by the spins in the zero-field plane is not affected by the gradient field. If the signal is phase detected at the Larmor frequency, ω_0, given by $\omega_0 = \gamma H_0$ where H_0 is the static uniform component of the field, then the spins in the zero-field plane produce a time-independent signal. However, regions of the sample away from the zero-field plane do experience a time-dependent field and thus produce a time-dependent signal. By selecting the time-independent component of the total signal, only the spins near the zero field are observed.

The limitation of the spectrometer sensitivity to the region of the zero-field plane can most easily be demonstrated for the cw technique. We first solve the Bloch equations for the magnetization in the presence of a sinusoidally time-dependent uniform magnetic field. If we assume a static homogeneous field, H_0, a low-level rf field, H_1, with frequency ω and in the x direction in the rotating frame, and a homogeneous time-dependent field, $H_m = h\cos(\omega_m t)$, the transverse component of the magnetization in the rotating frame expressed in complex notation is

$$M(t) = i\gamma H_1 M_0 \sum_{k=-\infty}^{\infty} \sum_{n=-\infty}^{\infty} J_k\left(\frac{\gamma h}{\omega_m}\right) J_n\left(\frac{\gamma h}{\omega_m}\right) \frac{\exp[-i(k-n)\omega_m t]}{1/T_2 + i(\delta\omega + n\omega_m)}. \tag{20}$$

Here $J_n(x)$ is the nth-order Bessel function of the first kind and $\delta\omega \equiv \gamma H_0 - \omega$. A similar expression was derived from the Bloch equations by Anderson for the problem of field-modulated cw NMR.[32] If the phase-detected signal, assumed proportional to $M(t)$, is averaged to remove the time-dependent components, then the signal is proportional to f where

$$f = i\gamma H_1 M_0 \sum_n J_n^2\left(\frac{\gamma h}{\omega_m}\right)\left(\frac{1}{T_2} + i(\delta\omega + n\omega_m)\right)^{-1}. \tag{21}$$

If a sinusoidally modulated linear gradient is assumed instead of the homogeneous field H_m, then h is replaced by Gx and Eq. (21) becomes a spatial response function showing the localization of the spectrometer sensitivity to the zero-field plane. If we simplify to the case where the homogeneous linewidth is much smaller than the modulation frequency, the resonance offset is zero, and the "in-phase" component of the signal is observed, then we obtain

$$f_y = \gamma H_1 T_2 M_0 J_0^2\left(\frac{\gamma G x}{\omega_m}\right). \tag{22}$$

The half-height width of the central portion of this response function, which is a measure of the "thickness" of the zero-field plane, is $2.2\omega_m/\gamma G$. The first sidebands are at $x = 3.8\omega_m/\gamma G$ and have an amplitude of 0.16 when the amplitude of the central portion is normalized to unity.

The above discussion is equally applicable to pulse techniques. If 90° rf pulses are applied with a pulse

separation T greater than T_1, if the free induction decay after each pulse is integrated, and if the pulses are asynchronous with respect to the field modulation, it can be shown that the average signal after many pulses is given by Eq. (21) with γH_1 replaced by $2\pi/T$.

Time-dependent gradient fields can limit the spectrometer sensitivity to a point, whereas uniform static gradients can only limit the sensitivity to a plane. If two orthogonal static gradients are applied simultaneously, the result is a third, intermediate, gradient which can still only limit the sensitivity to a plane. If two orthogonal time-dependent gradients, each with unique time dependence, are applied simultaneously, only the spins at the intersection of the two zero-field planes will experience a time-independent field. Thus the spectrometer sensitivity can be limited to a line by the application of two time-dependent gradients. Similarly, three orthogonal gradients, each with a unique time dependence, can be used to limit the sensitivity to a point. This point is referred to as the sensitive point.

The gradients used to produce the sensitive point can have almost any time dependence as long as it is different for each of the three gradients. Random or pseudo-random noise modulation of the gradient fields may be the most efficient in terms of response width for a given gradient strength, but attempts to use noise modulation resulted in "noisy" images. It is also possible to define a sensitive point with two time-dependent gradients and one static gradient. In this work, two of the orthogonal gradients had periodic time dependence with the same frequency but with a 90° phase difference between them. The third gradient was modulated at a different frequency.

The spatial response function for more than one time-dependent gradient field can be obtained by extending Eq. (22). Two orthogonal gradients having the same modulation frequency but a 90° phase shift between them can be considered as a single constant-amplitude gradient with rotating direction. The spatial response function for the resulting "zero-field line" is given by Eq. (22) with x replaced by r where r is the radial distance from the line defined by the intersection of the two zero-field planes. The spatial response function for two gradients having sinusoidal modulation at different frequencies can be obtained from the Bloch equations by starting with the homogeneous time-dependent field

$$H_m = h\cos(\omega_m t) + h'\cos(\omega'_m t).$$

The resulting equation equivalent to Eq. (22) is

$$f_y = \gamma H_1 T_2 M_0 J_0^2\left(\frac{\gamma Gx}{\omega_m}\right) J_0^2\left(\frac{\gamma Gy}{\omega_m}\right), \tag{23}$$

Thus two time-dependent gradients do limit the sensitivity to a line.

The sensitive point, located at the point of intersection of the zero-field planes of the three time-dependent gradients, can be moved anywhere in the sample by shifting the zero-field planes. The method used in this work to shift the zero-field planes will be discussed in Sec. III.

The uniformity and linearity of the field gradients are relatively unimportant in the production of a sensitive point. However, each gradient must have only one zero-field plane. For distortion-free images, the strength of the gradients in the neighborhood of the sensitive point must remain constant as the point is moved throughout the sample.

C. Pulses and gradients

If the SFP technique is used in the presence of a static linear field gradient, Gx, then Eq. (13) can be taken from the frequency domain to the spatial domain by replacing ϕ by γGxT. Thus a static gradient limits the spatial sensitivity of the SFP technique to a plane and produces a spatial response function with the shape shown in Fig. 1. The width of this response function is approximately $2\pi/\gamma GT$.

If the SFP technique is used in the presence of a time-dependent field gradient, the spatial response function is more difficult to determine. It can be calculated for some special cases, but a spatial response function for the SFP technique equivalent to Eq. (22), derived for the cw technique, will not be presented.

The SFP technique produces a continuous NMR signal by repeatedly refocusing the magnetization. It is not surprising that this coherent refocusing ability is easily destroyed by asynchronous variations in the magnetic field. Allerhand[33] has considered, in some detail, the effectiveness of field fluctuations in the destruction of the magnetization during the Carr-Purcell pulse sequence. The importance of field fluctuations in the destruction of the magnetization during the DEFT sequence has also been reported.[34]

One approach to the determination of the spatial response function is to consider the power spectrum of the phase-alternated SFP pulse sequence. Since the rf pulses alternate in phase, no net power is applied to the sample at the resonance frequency. The power is applied in a wide frequency spectrum of narrow lines spaced $1/T$ apart with the first sidebands $1/2T$ above and below the resonance frequency. If the amplitude of the field modulation experienced by a group of spins is large enough, the spins can absorb power from the first sidebands. Since the pulses are intense and closely spaced, the sidebands are strong enough to quickly "saturate" the spins. This sort of consideration provides a means of calculating a response function with a width somewhat less than that for the static gradient.

III. EXPERIMENTAL DETAILS

The measurements were made at 60 MHz using a modified Bruker B-KR 322s pulsed NMR spectrometer and an AEI RS2 current-regulated electromagnet. A simplified block diagram of the complete system is shown in Fig. 2. The underlined blocks are components of the Bruker spectrometer.

The trigger pulse source in Fig. 2 was a variable-frequency pulse generator which was normally set between 1 and 5 kHz. The timing of the trigger pulses, and thus the timing of the rf pulses, was not coherent with respect to the 60 MHz carrier. Experience indi-

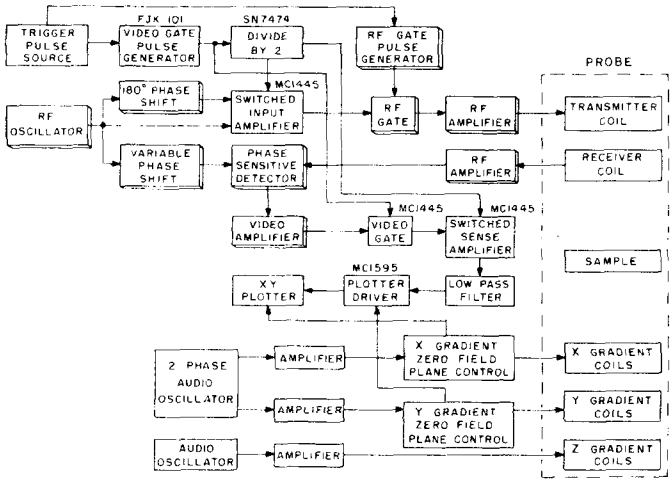

FIG. 2. Simplified block diagram of the electronics. The underlined blocks are part of the Bruker spectrometer upon which the system is based. The blocks with numbers above them represent single integrated circuits. FJK101 is a delay multivibrator, SN7474 is a type-D flip-flop, MC1445 is a gate-controlled two-channel-input wideband amplifier, and MC1596 is a balanced modulator-demodulator.

cated that this sort of coherence, or lack of it, did not affect the final signal.

The video-gate pulse generator, divide-by-two circuit, switched input amplifier, video gate, and switched sense amplifier were each single integrated circuits. The MC1445 integrated circuit, which was used for three of these units, has two sets of differential inputs and accepts a gate signal which determines which set of input signals is amplified. For the video gate, one set of inputs was grounded so that the video signal was amplified only when the gate signal was on. The video-gate pulse generator turned off the video gate at the start of the rf pulse and kept it off until a few microseconds after the end of the rf pulse. The video gate thus removed the large and unwanted signal produced by the rf pulse feedthrough.

The divide-by-two circuit changed state each time the video gate turned on. When this circuit changed state, the switched input amplifier, which was also a MC1445 integrated circuit, changed from amplifying one set of inputs to amplifying the other. Thus the rf pulses were phase alternated since one input signal was phase shifted 180° with respect to the other. The switched input amplifier operated at 30 MHz and was followed by a frequency-doubling circuit not shown in Fig. 2. The divide-by-two circuit also gated the switched sense amplifier. The signal from the video gate was fed into the positive half of the differential input of one input channel and the negative half of the other channel. Thus when the divide-by-two circuit changed state, the switched sense amplifier changed the sign of its amplification. This switched sense amplifier supplied the factor of $(-1)^n$ in Eq. (12). The two gated amplifiers driven by the divide-by-two circuit caused the spectrometer to operate as a chopper stabilized amplifier. These two amplifiers could be added to any pulsed NMR spectrometer to remove effects such as baseline drift and coherent logic noise.[35] Except for the five integrated circuits discussed above, the upper blocks in Fig. 2 represent a standard pulsed spectrometer and need no further explanation.

The low-pass filter, used to remove the high-frequency noise and unwanted time-dependent components of the signal, was a simple *RC* filter. The time constant, between 0.1 and 1 sec, was longer than the period of the gradient modulation but short enough so that the *xy* plotter responded with negligible distortion to the variation in signal as the position of the sensitive point was scanned through the sample.

Two audio oscillators were used to produce the signals for the time-dependent field gradients. The oscillator supplying the x and y gradients had two outputs with a 90° phase difference between them. The audio amplifiers driving the x and y gradient coils were the two halves of a home-built stereo amplifier which was capable of supplying 20 W per channel. For most of the images produced, the x and y gradient time dependence deviated significantly from a pure sine wave due to the severe overdrive of the audio amplifier. The audio oscillator for the x and y coils were normally set between 20 and 100 Hz and the oscillator for the z coils between 300 and 500 Hz. The final NMR signal seemed to have little dependence upon these frequencies. The frequency of the gradient modulation, the repetition rate of the rf pulses, and most other experimental parameters were chosen completely by trial and error.

The zero-field plane controls shifted the zero-field planes and thus the position of the sensitive point in the sample. The x gradient zero-field plane control was a clock motor and a pair of ganged potentiometers as shown in Fig. 3. The control simultaneously shifted the ratio of currents in the two halves of the x gradient coil set and the x position of the *xy* plotter pen The y gradient zero-field plane control was similar to the x control but ran at a much slower rate. Thus as the x control repeatedly scanned the sensitive point through the sample in the x direction, the y control slowly scanned the point through the sample once in the y direction The x scan was repeated every 10—100 sec and the vertical, y, scan was set to allow between 20 and 70 horizontal, x, scans per image.

The plotter driver combined the y position signal from the y gradient zero-field plane control and the

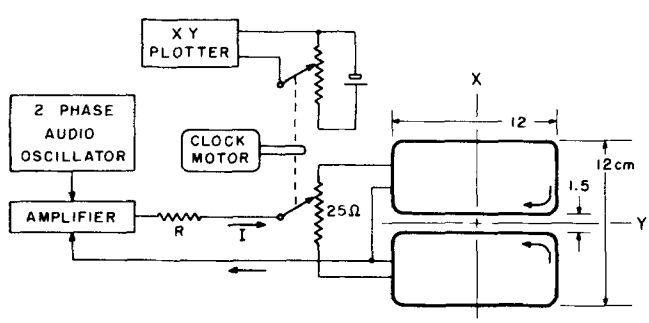

FIG. 3. Details of the x gradient coils and zero-field plane control. The pair of coils shown is wound completely in the scanning plane which is an *xy* plane. Each of the coils has a resistance of 11 Ω and contains 20 turns. The y gradient system is the same except for a 90° rotation of the gradient coils about the z axis.

video signal from the spectrometer. The plotter driver could operate in two modes. In the first, the two signals were simply added so that the resulting image consisted of a set of curves, each corresponding to a plot of signal amplitude versus x position in the sample. Each of these plots were offset vertically, or in the y direction, corresponding to the y position of the trace in the sample. In the second mode, the pen oscillated rapidly in the y direction with an amplitude proportional to the video signal. The average position of the pen was controlled by the y gradient zero-field plane control. In this mode of operation, the plotter driver was a balanced modulator-integrated circuit with the carrier signal of about 10 Hz supplied by a third audio oscillator and the modulation signal supplied by the low-pass filter.

For simplicity, the probe was designed to provide a sensitive point which could be moved in only two dimensions, x and y, and was fixed in the third. In order to change the z position of the sensitive point, the sample was moved. The volume available for the sample was a cylinder with axis in the z direction, the direction of the H_0 field. This volume was 7.5 mm in diameter and about 4 cm long. The plane to which the sensitive point was constrained, the "scanning plane", was normal to the cylinder axis. The receiver and transmitter coils were both "saddle shaped" and were wound so that their fields were orthogonal. The receiver coil was wound on the thin wall glass tube enclosing the sample volume and had a length roughly equal to the diameter. The transmitter coil had a diameter of 12 mm and was wound with the saddle coil geometry prescribed by Ginsberg and Melchner[36] to provide optimum rf homogeneity. The 90° pulse length was about 15 μsec.

The z gradient coils were a pair of Helmholtz coils wound in opposition with a coil separation of about 11 mm. The pair were equally spaced above and below the scanning plane and coaxial with both the sample volume cylinder and the field H_0. The z coils accurately restricted the sensitive point to the scanning plane.

Each of the x and y gradient coil sets was a pair of flat rectangular coils wound in the scanning plane. The geometry of the x coil pair is shown in Fig. 3. The y coil pair was identical but rotated about the z axis by 90°. Each gradient was produced by the pair of wires close to the sample, one on each side, in the scanning plane. The return path for the current was kept well away from the sample so its contribution to the field could be neglected. Each coil contained 20 turns.

The position of the zero-field plane produced by the x gradient coil pair was linearly related to the position of the x control potentiometer shown in Fig. 3. If θ is the position of the potentiometer dial with $\theta = \pm 1$ at the extreme settings and $\theta = 0$ at the center, and if the coordinate system of the sample volume is defined so that $x = \pm a$ at the wires and $x = 0$ at the center, than the Biot-Savart law gives the position, x_0, of the zero-field line in the scanning plane as

$$x_0 = \frac{a}{1 + 2R_c/R_p}\theta, \tag{24}$$

where R_c is the resistance of each half of the x coil pair and R_p is the total resistance of the potentiometer. Thus with the simple system of Fig. 3 used for both the x and y gradient center controls, the positions of the sensitive point and the xy plotter pen are linearly related and very little spatial distortion is produced. Each coil of the coil pairs had a resistance of 11 Ω, the wire separation was 15 mm, and the control potentiometer resistance was 25 Ω. With these values, Eq. (24) gives ± 4 mm for the total range of the sensitive point.

With this parallel wire gradient coil geometry, the strength of the gradient at the zero-field line is

$$G(x_0) = \frac{IN}{2\pi}\frac{a^2 + 3x_0^2}{(a^2 - x_0^2)^2} \tag{25}$$

with N the number of turns in each coil and I the sum of the currents through both. Equation (25) is in SI units. The gradient strength when the zero-field line is at the center of the sample volume is approximately $0.16IN/a^2$. For comparison, the field gradient at the center of a Helmholtz pair wound in opposition and with equal currents, $\frac{1}{2}I$, in each coil is approximately $0.11IN/a^2$ with $2a$ the separation between the coils. Thus the parallel-wire geometry produces a gradient strength similar to that of a Helmholtz pair with equivalent geometry. The current I in the actual measurements was limited by the output voltage of the audio amplifier and had a maximum value of about 750 mA. This produced a maximum x gradient strength at the center of the sample of about 5 G/cm.

The gradient strength and the sensitive-point size depend upon the position of the point in the scanning plane if the simple zero-field plane control shown in Fig. 3 is used. If the resistor R in Fig. 3 has a high value, the current I is independent of the potentiometer setting. Assuming the width of the sensitive point is inversely proportional to the gradient strength, Eq. (25) indicates that the sensitive point is narrower at the edges of the sample volume than at the center. The distortion in the image due to this positional dependence of the sensitive-point size is evident in some of the images presented in Sec. IV. This distortion could be reduced, at the expense of simplicity, by making the gradient currents dependent upon the sensitive-point position.

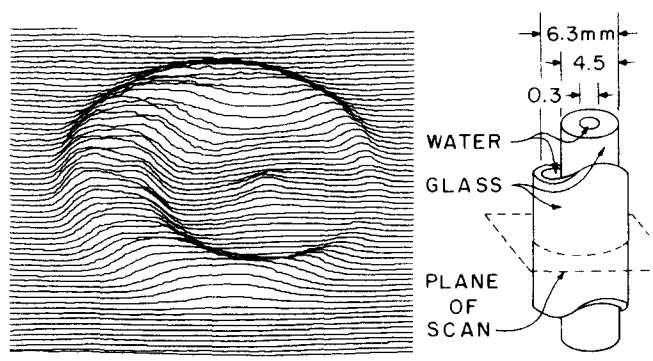

FIG. 4. xy plotter trace produced by the sensitive-point method. The image represents a thin cross section through a glass tube containing water and a thick wall glass capillary. The distance over which the center traces go from zero to maximum can be used to estimate the spatial resolving power of the system. In the following images, the scanning plane is normal to the axis of the sample as shown here.

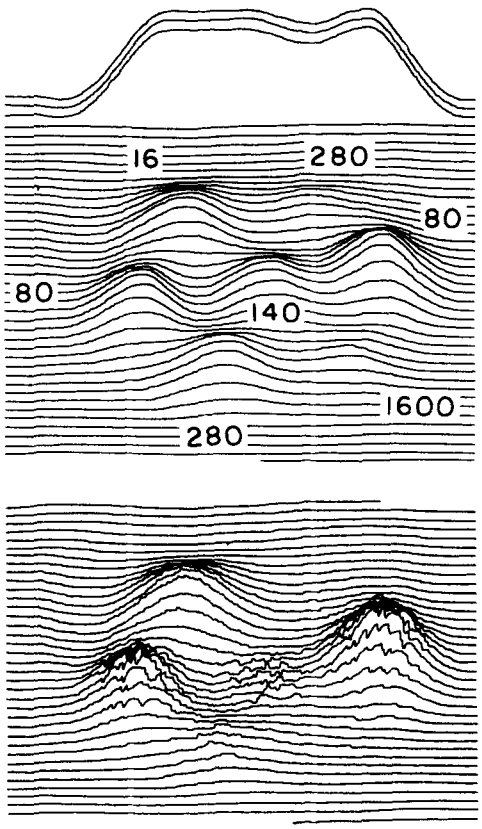

FIG. 5. A cross section of seven glass tubes each filled with water. The numbers are the T_1 values in msec. The bottom image shows the effect of adding an 180° rf pulse every 100 msec during the scan. Note that the effect of the saturating pulses depends upon the T_1 of the sample. The three traces above the top image represent a projection of the image and were produced by turning off the y, or vertical, gradient field.

IV. RESULTS

This section displays some of more than 70 images produced during a two-week period by the equipment described in Sec. III. All of the images shown are unretouched copies of the xy plotter output. They are images of thin sections and not projections. The images were recorded using the 60-MHz proton signal.

The sample used for Fig. 4 was a thick wall glass capillary inside a glass tube with the capillary and the space between the tubes filled with water. The axis of the cylindrical sample volume of the probe and the axes of the glass tubes of Fig. 4 were in the direction of H_0 which was horizontal. In Fig. 4 and in the following images, the left-hand side of the image corresponds to the top of the actual sample. The image in Fig. 4 gives a reasonable measure of the capabilities of the system. The resolution can be estimated from the shape of the individual traces since the amplitude of each trace is proportional to the signal and thus to the amount of water. The center traces on the left-hand side of the image go from about 20 to 80% in roughly 0.3 mm, which we take as a measure of the spatial resolution. At the outer edge of the capillary, the traces show a slightly more gentle slope indicating that the diameter of the sensitive point is smaller at the edges of the image than at the center. There is no measurable spatial distortion in the image. However, the y gain of the plotter was made slightly less than the x gain in order to make the image appear more like a raised surface viewed at an angle.

The horizontal scan time used for the image in Fig. 4 was 120 sec. If an independent point is assumed every 0.3 mm, there are about 28 independent points per scan. Thus this image can be characterized as having about 800 independent points, a data collection time per point of about 4 sec, and a signal-to-noise ratio of about 10. This image was produced with a z gradient strength of 2 G/cm and modulation frequency of 400 Hz. The x and y gradients had a strength of 4 G/cm and modulation frequency of 57 Hz. The rf pulses were 2 μsec in length, corresponding to about 30°, and had a repetition frequency of 3 kHz. The video-gate length was 100 μsec. The total time for the image formation was 2 h.

The width of the spatial response function given by $2\pi/\gamma GT$, which would be expected for a static gradient, is 1.8 mm which is significantly larger than the observed width of 0.3 mm. This discrepancy indicates that a calculation of the width is needed which includes the effect of the gradient time dependence.

Figure 5 shows two images of the same sample. The sample was a bundle of seven roughly equivalent small glass tubes each filled with water. The water in each of the tubes was doped with different amounts of $MnCl_2$ in order to give differing longitudinal relaxation times. The T_1 of the water in each tube is indicated in milliseconds on the upper image. The only difference in the two images of Fig. 5 was the addition of an 180° rf pulse every 100 msec during the production of the lower image. These saturating pulses were asynchronous with respect to the rf pulses and the modulating gradients. The saturating pulses destroyed the signal from the long T_1 samples, modulated the signal from the intermediate T_1 samples, and did not significantly affect the signal from the short T_1 samples.

For the top three traces of Fig. 5, the y gradient field was turned off with nothing else changed. These curves are the projection of the slice along the vertical direction of the image. This projection seems to contain little information about the distribution of the sample and indicates the difficulty that can be encountered in reconstructing an image from a set of projections.

For Fig. 5, the gradient strength was reduced in order to increase the sensitive-point volume and thus improve the signal-to-noise ratio. As a result, the 20–80% distance measured from the image is slightly over 0.5 mm. The upper image contains 300 independent points with a signal-to-noise ratio of about 50. The time per point was about 4 sec. The rf pulse rate was 6 kHz and the time per sweep was 64 sec but otherwise the settings were similar to those used for Fig. 4.

Figure 6 shows the water distribution in a fresh spring onion. The image represents a thin cross section near the roots. The relatively dry outer rings and wet central region are clearly visible. Figure 7 is identical to Fig. 6 except that it was taken two days later and with higher spectrometer gain. Only half of the traces

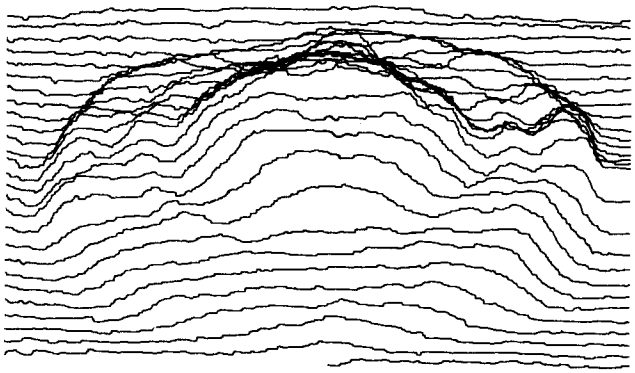

FIG. 6. The image of a thin cross section near the roots of a reasonably fresh spring onion. The apparent height of the image is proportional to the density of free water at the corresponding point in the sample. The outer rings and wet central region are clearly visible.

were recorded since the curves for the top half of the image would have traced over those shown. Note that there is more water near the right-hand side of the image which corresponds to the bottom of the sample. Figure 7 demonstrates the large dynamic range possible with this technique.

In complex samples such as an onion, the NMR signal produced by the SFP technique is principally a measure of the free water. The short T_2 of the protons in the tightly bound water and in other rigidly bound molecules limits their contribution to the observed signal. The details in the image of the onion were observed to depend upon the rf pulse length but did not change with the addition of repetitive 180° saturating pulses. According to the discussion in Sec. IIA, and in particular Eq. (14), this behavior seems to indicate that T_2 is not constant throughout the onion.

The following images were produced with the second mode of display in which the plotter pen vibrated with an amplitude proportional to the video signal. This

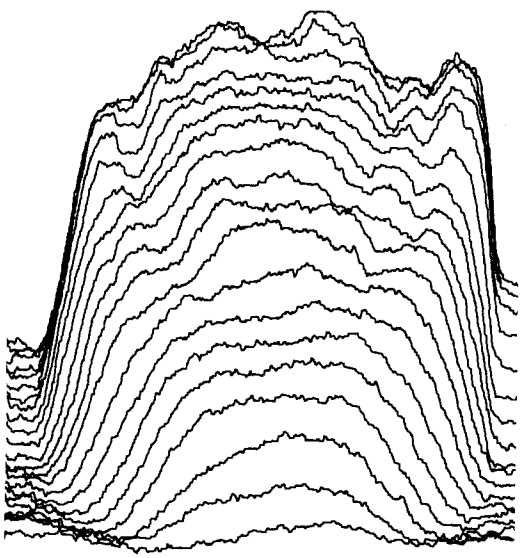

FIG. 7. The same onion as in Fig. 6 but two days older. The system gain has been considerably increased in order to bring out the details and the change in water distribution. Only half of the full image was plotted in order to prevent confusion.

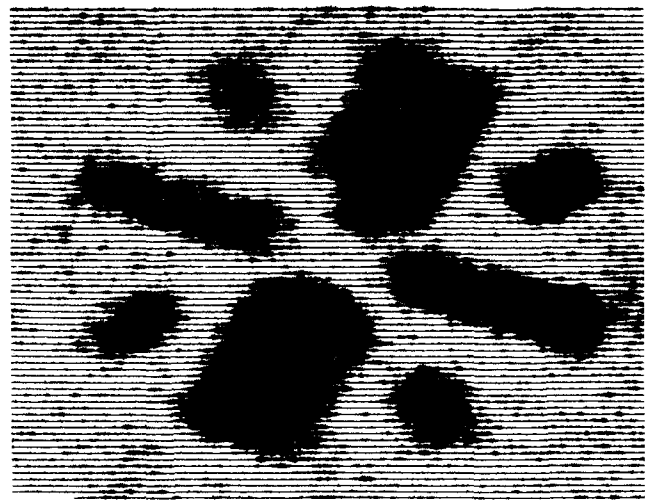

FIG. 8. The image of water loaded into a 7-mm-diam Teflon rod. Two 2.0-mm- and six 1.1-mm-diam holes were drilled into the rod from around the periphery and filled with water. The plotter pen vibrated vertically during each trace with an amplitude proportional to the video signal. Thus the water appears black and the Teflon, which contains no protons, is not seen. The vertical gain of the plotter was slightly less than the horizontal, giving the rod a compressed appearance.

method did not have the dynamic range or the linearity of the first mode but did produce images that are easier to interpret. The contrast and brightness of the image were controlled by adjustments in the plotter driver.

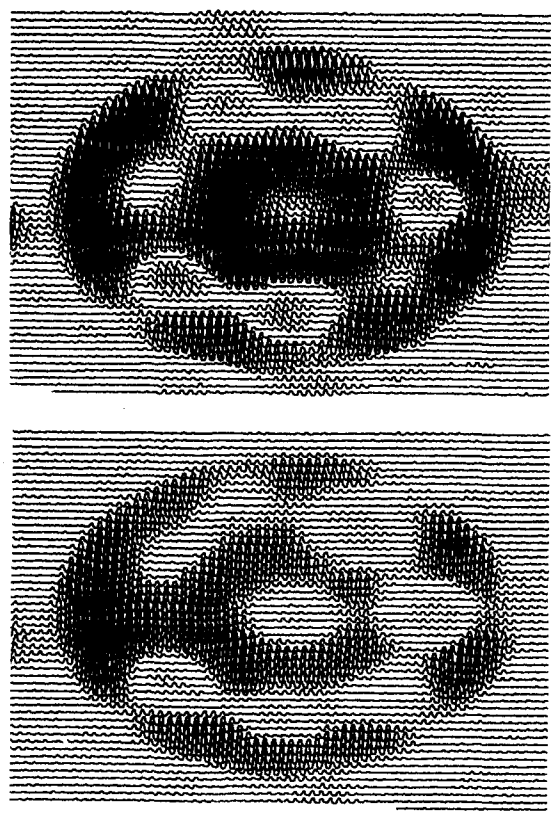

FIG. 9. Images of a glass tube filled with water and packed with 2-mm-diam glass balls. The sample was displaced 0.5 mm along its axis between the two "photographs". These two images can be combined to locate the glass balls in three dimensions.

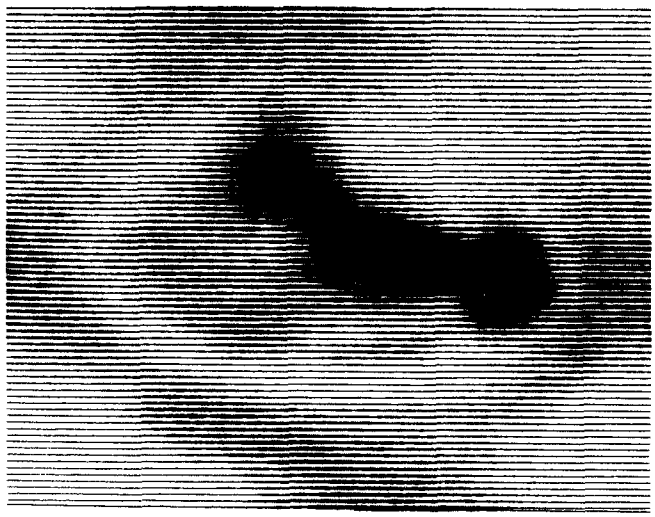

FIG. 10. Cross section of a chicken wing bone. The light ring is the bone, the dark areas outside are traces of flesh not cleaned from the bone, and the dark central region is the marrow. The mode of display used in this image does not allow the dynamic range that is exhibited, for example, in Fig. 7. At the center of the marrow, the intensity information is lost as the lines merge to form solid black.

Figure 8 is the image of a thin cross section through a 7-mm-diam Teflon rod. Holes were drilled into the rod from around its circumference and filled with water. The holes were 2.0 and 1.1 mm in diameter. A small air bubble or Teflon chip can be seen at the bottom of the upper large hole. The "slice" thickness was much less than the diameter of the holes. The only measurable distortion in the image results from the unequal x and y plotter gains.

Figure 9 shows two views of a glass tube filled with water and 2-mm-diam glass balls. The two images are cross sections of the same sample but displaced by 0.5 mm along the z direction. The two taken together establish the location of the balls in three dimensions.

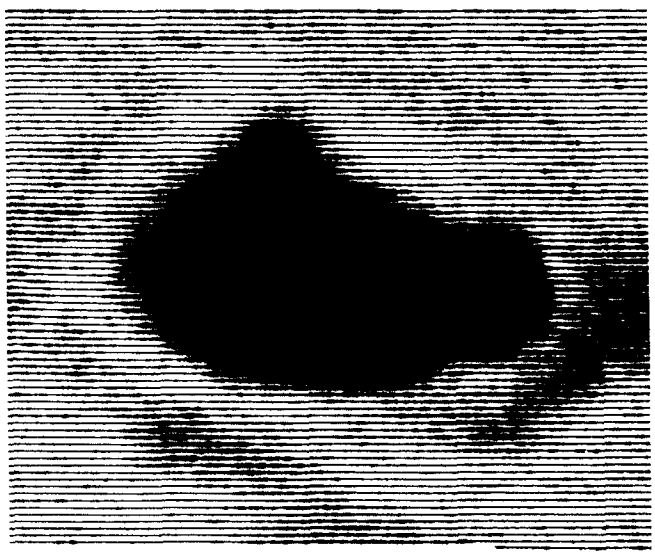

FIG. 11. This image is identical to Fig. 10 except for the spectrometer settings. The difference in the appearance of the marrow is thought to be due to the discrimination against the short T_2 components of the signal in this image.

If the two images were superimposed with each printed in a different color and the result viewed with a prism in front of one eye, the image would appear to have depth, and the location of the balls in the third dimension could be more readily determined. For these two images, the pen modulation frequency was slowed in an attempt to reduce the contrast and improve the display linearity.

Figures 10 and 11 are images of a chicken wing bone. They represent a cross section near the small end of the ulna and show the internal marrow and slight traces of flesh on the outer surface. Figure 10 was taken with a 80-μsec video gate and Fig. 11 with a 150-μsec video gate and higher spectrometer gain. Both were produced with a 3.6-kHz rf pulse rate, 32-sec horizontal scan, and 30° rf pulse. The change in the video-gate length changed the appearance of the marrow. Although the effect of the gate length on the image of a complicated sample is not understood, it is reasonable to assume that the longer video gate caused the spectrometer to ignore the signal from regions with shorter T_2 relaxation times. The images of simple liquid samples, such as the sample used for Fig. 5, did not depend upon the video gate time.

Figure 12 is a cross-sectional image of a glass tube filled with water and containing an ordinary fillister head brass screw. The screw was tilted at a slight angle giving the head an oval appearance. This image shows the insensitivity of the sensitive-point method to nonuniformities in the applied fields.

V. DISCUSSION

The weakness of the NMR signal is the most important factor limiting the sensitive-point imaging technique and perhaps all NMR imaging techniques. Image

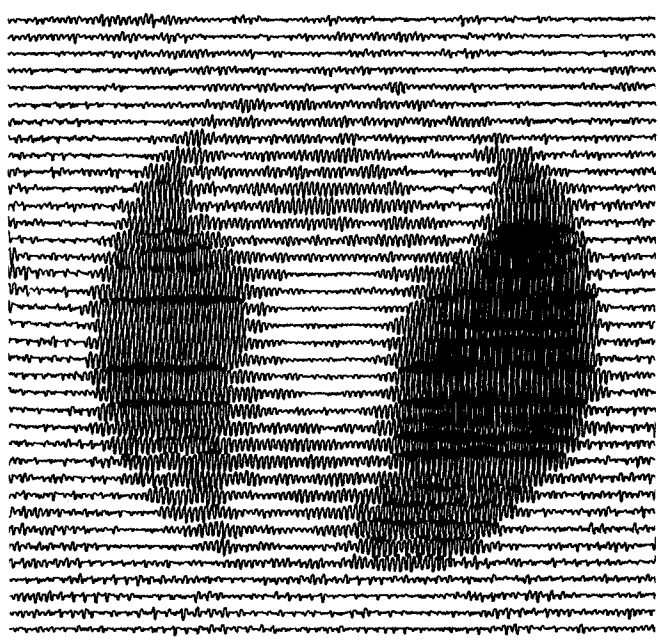

FIG. 12. Cross section through a glass tube containing water and a fillister head brass machine screw. The screw is slightly tilted giving an oval shape to the head. This image clearly indicates the insensitivity of the sensitive-point method to H_0 and H_1 inhomogeneities.

distortion and other problems can be ameliorated by careful design, but the three related parameters of image noise, resolution, and data collection time are strictly limited by the signal-to-noise ratio of the resonance signal. The limitations imposed upon the sensitive-point image formation method by noise considerations can be estimated. Abragam gives an order-of-magnitude calculation for the voltage signal-to-noise ratio obtainable by cw magnetic resonance assuming negligible inhomogeneity broadening and $T_1 = T_2$.[37] The ratio, assuming the SFP technique and observing protons in water at room temperature, becomes

$$\frac{S}{N} = \frac{V_s}{10f}\left(\frac{H_0^3 Q\theta}{2V_c}\right)^{1/2}. \tag{26}$$

In this expression for S/N, θ is the integrating time constant in seconds, V_s and V_c are the volumes in cm^3 of the sensitive point and receiver coil, respectively, and Q is the Q of the sample coil tank circuit. The factor f takes into account the noise introduced by the apparatus and is unity if the apparatus is noise free. For the equipment used in this work, $Q = 70$, $V_c = 0.6$ cm^3, $H_0 = 14$ kG, and $\theta = 0.1$ sec. With these numbers, Eq. (26) becomes

$$S/N = 4 \times 10^5 V_s/f.$$

Thus f is roughly 1.1 if the values of S/N and V_s are obtained from the experimental images of Sec. IV. Although f is fortuitously low, the low value does indicate that no dramatic improvement in the images produced by the sensitive-point method can be expected by improving the spectrometer.

Increasing the resolution of the images is expensive in terms of time. Equation (26) indicates that the averaging time is proportional to the inverse sixth power of the sensitive-point diameter if the signal-to-noise ratio remains constant. Thus decreasing the resolution distance of the image in Fig. 4 from 0.3 to 0.1 mm would require increasing the integration time constant from 0.1 sec to over 1 min. Thus a reasonable value for the lower limit to the resolution distance is on the order of 0.1 mm. This limit might be lowered by going to high magnetic fields, low sample temperatures, small samples, and long averaging times.

Increasing the size of the sample volume would make the NMR imaging technique more useful for some medical applications. If the receiver coil diameter is increased to 50 cm and the field decreased to 1 kG, Eq. (26) becomes

$$S/N = 3 \times 10^3 V_s \theta^{1/2}. \tag{27}$$

This equation is based on the assumption, which may prove unrealistic, that Q and f do not increase. For the same signal-to-noise ratio and the same integrating time constant, Eq. (27) indicates that the resolution distance increases by a factor of 7.5. Equation (27) also indicates that images could be produced with the same signal-to-noise ratio, number of independent points, and data collection time as the ones displayed in Sec. IV but with the over-all dimensions increased from 8 mm to 6 cm and the resolution distance increased from 0.3 to 2.3 mm.

Multiple sideband detection is a modification of the sensitive-point method which would decrease the data collection time and ease the limits imposed by signal-to-noise considerations. The long string of short closely spaced rf pulses used in the SFP technique has a wide range of narrow sidebands in the frequency domain. In this work, the signal occurring between two of the sidebands produced by the pulses was detected. If one of the three gradients is made time independent, the signal between each sideband contains information about the sample density at a different region of the sample. If several phase detectors are used, each detecting a different signal sideband, the output of each detector is proportional to the sample density at a different place along the static gradient. With multiple sideband detection, the time required to produce an image would be decreased by a factor equal to the number of detectors used. Thus "real time" display of the image on a slow phosphor CRT becomes a possibility for low-resolution images.

Combining the Fourier transform technique with the time-dependent gradient technique is a modification which is related to multiple sideband detection and has the same objective. One of the many ways to combine the techniques is to restrict the spatial sensitivity to a line by applying two time-dependent gradients, apply a static gradient along that line, and determine the distribution of the sample along the line by using pulse Fourier transform techniques. The rf pulses are applied at intervals of about T_1 and are asynchronous with respect to the time dependence of the two gradients. The free induction decay after each pulse is recorded. The average of these free induction decays is Fourier transformed to give the sample distribution on the selected line. By moving the selected line and repeating the process, an image is developed. A similar method using selective irradiation and switched gradients has been attempted by others.[10,17] A simple estimate of the relative signal-to-noise ratios of the Fourier transform and scanned point methods indicates that the former obtains the sample distribution along the line in roughly the same time the latter obtains one point. This estimate, however, is based on the assumption of ideal conditions for the Fourier transform. It is assumed that T_1 is known and is the same for all parts of the sample and that the static gradient strength and rf pulse interval are optimally set. It is also assumed that there are no broadening mechanisms other than the static gradient and the intrinsic T_2 broadening. Thus in practice, the advantage may be less than dramatic. One disadvantage of the Fourier transform modification is that it forfeits the considerable advantages of the SFP technique such as insensitivity to the magnetic field. The added complexity of the transform computation and the added demands upon field stability and uniformity may outweigh any advantage gained in speed.

It is difficult to compare the sensitive-point method of image formation with the image reconstruction method without examining the latter in detail, which is beyond the scope of this paper. Perhaps the only valid test of any method of NMR image formation is the quality of the images produced.

The ability to make measurements at a selected region of the sample is one distinct advantage of the sensitive-point method over the reconstruction methods. For example, with the system used in this work, after an image of the density distribution is produced and the plotter pen is raised, the zero-field plane controls can be manually adjusted to position the pen over a particular point in the image. The sensitive point is then accurately located in the corresponding region of the sample. A quick and accurate determination of T_1 using the method described in Sec. II can be made, or a more detailed image of the small area of interest can be produced.

A wide range of applications and variations of the sensitive-point technique should be possible. For example, pulsed NMR flow measurement techniques[38,39] can be modified to measure and monitor macroscopic flow as a function of location in the sample. Also, if the field H_0 could be carefully controlled in the presence of the time-dependent gradients, the time sharing or cw technique could be used to obtain the high-resolution spectrum as a function of position.

VI. CONCLUSIONS

Useful NMR images of the free water distribution in complex heterogeneous samples can be produced by the sensitive-point method. A rough estimate of the signal-to-noise ratio of the images in terms of the size of the sensitive point, averaging time per point, and other experimental parameters is given by Eq. (26). For the images displayed, $S/N \approx 120\, d^3 \theta^{1/2}$, where d is the resolution distance in mm and θ is the signal averaging time per point in sec. Equation (26) indicates that, if the engineering problems can be surmounted, images can be obtained from samples on the order of 30 cm in diameter in a reasonable data collection time. The lower limit of the resolution distance is controlled by considerations of the signal-to-noise ratio and is about 0.1 mm unless special techniques such as very high fields and multiple sideband detection are employed.

The sensitive-point imaging method is based upon two techniques. Time-dependent field gradients are used to spatially control the spectrometer sensitivity, and the SFP technique is used to produce a large continuous nuclear resonance signal. Using these techniques, a resolution distance for protons of about $0.4/GT$ mm was obtained where G is the peak gradient strength in G/cm and T is the interval between the rf pulses in msec. The signal produced by the phase-alternated SFP pulse sequence, as calculated from the Bloch equations, is proportional to f_y given by Eq. (13).

The ability to produce NMR images of a sample and to perform NMR measurements in selected regions of a sample should make NMR a still more valuable research tool. The signal-to-noise ratio limitation makes NMR images slower to produce than x-ray images. However, the power of NMR to provide a wide range of detailed information suggests NMR imaging may have a future.

ACKNOWLEDGMENTS

The experiment reported here was performed at the University of Nottingham with the encouragement, hospitality, and equipment of Professor E.R. Andrew. Many of the ideas presented were contributed by Dr. W.S. Moore. The paper was written at the University of Pittsburg with the hospitality of Professor I.J. Lowe. The author also benefited from many helpful discussions with Dr. A.N. Garroway and Professor P.C. Lauterbur.

*Supported in part by the National Science Foundation (GP-32861).

†Present address: Department of Physics, University of Nottingham, Nottingham NG7 2RD, England.

[1]R.V. Damadian, Science 171, 1151 (1971).
[2]D.P. Hollis, L.A. Saryan, J.S. Economou, J.C. Eggleston, J.L. Czeisler, and H.P. Morris, J. Natl. Cancer Inst. 53, 807 (1974).
[3]W.R. Inch, J.A. McCredie, R.R. Knispel, R.T. Thompson, and M.M. Pintar, J. Natl. Cancer Inst. 52, 353 (1974).
[4]R.R. Knispel, R.T. Thompson, and M.M. Pintar, J. Magn. Reson. 14, 44 (1974).
[5]L.A. Saryan, D.P. Hollis, J.S. Economou, and J.C. Eggleston, J. Natl. Cancer Inst. 52, 599 (1974).
[6]R.T. Pearson, I.D. Duff, W. Derbyshire, and J.M.V. Blanchard, Biochim. Biophys. Acta 362, 188 (1974).
[7]P.P. Mahendroo, D.R. Woodhouse, W. Derbyshire, and S.M.A. Baghdadi, *Proceedings of the 18th Ampere Congress*, Nottingham, edited by P.S. Allen, E.R. Andrew, and C.A. Bates (North-Holland, Amsterdam, 1975), Vol. 1, p. 285.
[8]P.C. Lauterbur, Bull. Am. Phys. Soc. 18, 86 (1972).
[9]P.C. Lauterbur, Nature 242, 190 (1973).
[10]P.C. Lauterbur, C.S. Dulcey, C.M. Lai, M.A. Feiler, W.V. House, D. Kramer, C.N. Chen, and R. Dias, in Ref. 7, Vol. 1, p. 27.
[11]P. Mansfield and P.K. Grannell, J. Phys. C 6, L422 (1973).
[12]P. Mansfield, P.K. Grannell, and A.A. Maudsley, in Ref. 7, Vol. 2, p. 431.
[13]J.M.S. Hutchinson, J.R. Mallard, and C.C. Goll, in Ref. 7, p. 283.
[14]P.R. Locher (private communication).
[15]P. Mansfield and P.K. Grannell, Phys. Rev. B 12, 3618 (1975).
[16]A. Kumar, D. Welti, and R.R. Ernst, J. Magn. Reson. (to be published).
[17]A.N. Garroway, P.K. Grannell, and P. Mansfield, J. Phys. C 7, L457 (1974).
[18]P.R. Smith, T.M. Peters, and R.H.T. Bates, J. Phys. A 6, 361 (1973).
[19]W.S. Hinshaw, Phys. Lett. A 48, 87 (1974).
[20]W.S. Hinshaw, in Ref. 7, Vol. 2, p. 433.
[21]H.Y. Carr, Phys. Rev. 112, 1693 (1958).
[22]A. Schwenk, J. Magn. Reson. 5, 376 (1971).
[23]A. Abragam, *The Principles of Nuclear Magnetism* (Oxford U.P., Oxford, 1961), Chap. 3, p. 44.
[24]R.R. Ernst and W.A. Anderson, Rev. Sci. Instrum. 37, 93 (1966).
[25]R. Freeman and H.D.W. Hill, J. Magn. Reson. 4, 366 (1971).
[26]R.L. Streever and H.Y. Carr, Phys. Rev. 121, 20 (1960).
[27]P. Waldstein and W.E. Wallace, Rev. Sci. Inst. 42, 437 (1971).
[28]T.C. Farrar and E.D. Becker, *Pulse and Fourier Transform NMR* (Academic, New York, 1971), Chap. 5, p. 80.
[29]Dinesh, M.T. Rogers, and G.D. Vicers, Rev. Sci. Instrum. 43, 555 (1972).
[30]J.S. Waugh, J. Mol. Spectrosc. 35, 298 (1970).
[31]W.E. Wallace, J. Chem. Phys. 54, 1425 (1971).
[32]W.A. Anderson, Phys. Rev. 102, 151 (1956).
[33]A. Allerhand, Rev. Sci. Instrum. 41, 269 (1970).
[34]R.R. Shoup and E.D. Becker, J. Magn. Reson. 8, 298 (1972).
[35]J.T. Gerig, G.B. Matson, and A.D. Stock, J. Magn. Reson. 15, 382 (1974).
[36]D.M. Ginsberg and M.J. Melchner, Rev. Sci. Instrum. 41, 122 (1970).
[37]A. Abragam, in Ref. 23, Chap. 3, p. 83.
[38]R.J. Hayward, K.J. Packer, and D.J. Tomlinson, Mol. Phys. 23, 1083 (1972).
[39]A.N. Garroway, J. Phys. D 7, L159 (1974).